Crystal structures of bovine milk xanthine dehydrogenase and xanthine oxidase: Structure-based mechanism of conversion

Cristofer Enroth*†‡, Bryan T. Eger‡§, Ken Okamoto‡¶, Tomoko Nishino‖, Takeshi Nishino¶, and Emil F. Pai*§**††**

*Ontario Cancer Institute/Princess Margaret Hospital, Division of Molecular and Structural Biology, 610 University Avenue, Toronto, ON, Canada M5G 2M9; University of Toronto, Departments of §Biochemistry, ††Medical Biophysics and Molecular and Medical Genetics and The Protein Engineering Network of Centres of Excellence, 1 King's College Circle, Toronto, ON, Canada M5S 1A8; ¶Nippon Medical School, Department of Biochemistry and Molecular Biology, 1-1-5 Sendagi, Bunkyo-ku, Tokyo 113-8602, Japan; and ‖Yokahama City University School of Medicine, Department of Biochemistry, Fukuura 3-9, Yokahama 236-0004, Japan

Communicated by Vincent Massey, University of Michigan Medical School, Ann Arbor, MI, July 26, 2000 (received for review June 1, 2000)

Mammalian xanthine oxidoreductases, which catalyze the last two steps in the formation of urate, are synthesized as the dehydrogenase form xanthine dehydrogenase (XDH) but can be readily converted to the oxidase form xanthine oxidase (XO) by oxidation of sulfhydryl residues or by proteolysis. Here, we present the crystal structure of the dimeric (M_r, 290,000) bovine milk XDH at 2.1-Å resolution and XO at 2.5-Å resolution and describe the major changes that occur on the proteolytic transformation of XDH to the XO form. Each molecule is composed of an N-terminal 20-kDa domain containing two iron sulfur centers, a central 40-kDa flavin adenine dinucleotide domain, and a C-terminal 85-kDa molybdopterin-binding domain with the four redox centers aligned in an almost linear fashion. Cleavage of surface-exposed loops of XDH causes major structural rearrangement of another loop close to the flavin ring (Gln 423—Lys 433). This movement partially blocks access of the NAD substrate to the flavin adenine dinucleotide cofactor and changes the electrostatic environment of the active site, reflecting the switch of substrate specificity observed for the two forms of this enzyme.

Milk xanthine oxidase is an archetypal enzyme, which was originally described as aldehyde oxidase in 1902 (1) and has since served as a benchmark for the whole class of complex metalloflavoproteins (2). Xanthine oxidoreductase enzymes have been isolated from a wide range of organisms, from bacteria to man, and catalyze the hydroxylation of a wide variety of purine, pyrimidine, pterin, and aldehyde substrates. All of these proteins have similar molecular weights and composition of redox centers (3, 4). The mammalian enzymes, which catalyze the hydroxylation of hypoxanthine and xanthine, the last two steps in the formation of urate, are synthesized as the dehydrogenase form xanthine dehydrogenase (XDH) and exist mostly as such in the cell but can be readily converted to the oxidase form xanthine oxidase (XO) by oxidation of sulfhydryl residues or by proteolysis. XDH shows a preference for NAD^+ reduction at the flavin adenine dinucleotide (FAD) reaction site, whereas XO fails to react with NAD^+ and exclusively uses dioxygen as its substrate, leading to the formation of superoxide anion and hydrogen peroxide (3). The enzyme is a target of drugs against gout and hyperuricemia (5), and the conversion of XDH to XO is of major interest as it has been implicated in diseases characterized by oxygen-radical-induced tissue damage, such as postischemic reperfusion injury (6). Recent work suggests that XO also might be associated with blood pressure regulation (7).

The active form of the enzyme is that of a homodimer of molecular mass 290 kDa, with each of the monomers acting independently in catalysis. Each subunit contains one molybdopterin cofactor, two spectroscopically distinct [2Fe-2S] centers, and one FAD cofactor. The oxidation of xanthine takes place at the molybdopterin center (Mo-pt) and the electrons thus introduced are rapidly distributed to the other centers by intramolecular electron transfer (8). The reduction of the natural oxidant substrate NAD^+ occurs through FAD. In contrast to other hydroxylases, XDH uses a water molecule as the ultimate source of oxygen incorporated into the product.

The full amino acid sequences of xanthine oxidoreductase enzymes from various sources have been deduced by sequencing of the respective cDNAs or genes. They all consist of approximately 1,330 amino acids and are highly homologous with, e.g., the bovine milk enzyme (1,332 residues) showing 90% sequence identity to the human liver enzyme (1,333 residues) (3, 9, 10). Limited proteolysis of mammalian XDH with trypsin cleaves the enzyme into three fragments of 20 kDa, 40 kDa, and 85 kDa, concomitantly converting it to XO (3). Comparative sequence alignment indicated that the two iron sulfur centers were located in the N-terminal 20-kDa fragment, FAD in the intermediate 40-kDa fragment, and the molybdenum center in the C-terminal 85-kDa fragment (3).

Small crystals of XO first were obtained during purification of the enzyme from bovine milk although they were not of sufficient quality to allow meaningful analysis (11). In the absence of structural information on either form of xanthine oxidoreductase, structure–mechanism correlations for this enzyme have been inferred from the distantly related enzymes aldehyde oxidase (ALO) from *Desulfovibrio gigas* (23% identity for the FeS- and Mo-pt-domains; ALO lacks a flavin cofactor domain) (12, 13) and CO dehydrogenase (COD) from *Oligotropha carboxidovorans* (17% identity over all its three S, M, and L subunits) (14). Although this approach provided good models of the reaction mechanism, especially for the Mo-pterin subsite (4, 13), there was little information available on the FAD site. Obviously, nothing was known on the structural changes accom-

Abbreviations: ALO, aldehyde oxidase from *Desulfovibrio gigas*; COD, CO dehydrogenase from *Oligotropha carboxidovorans*; Mo-pt, molybdopterin phosphate; XDH, xanthine dehydrogenase; XO, xanthine oxidase; FAD, flavin adenine dinucleotide.

Data deposition: The atomic coordinates have been deposited in the Protein Data Bank, www.rcsb.org (1FO4 for XDH and 1FIQ for XO).

†Present address: University of Skovde, Department of Natural Sciences, Box 408, S-54128 Skovde, Sweden.

‡C.E., B.T.E., and K.O. contributed equally to this work.

**To whom correspondence and reprint requests should be addressed. E-mail: pai@hera.med.utoronto.ca (E.F.P.) or nishino@nms.ac.jp (T.N.).

The publication costs of this article were defrayed in part by page charge payment. This article must therefore be hereby marked "*advertisement*" in accordance with 18 U.S.C. §1734 solely to indicate this fact.

Table 1. Statistics for data collection and refinement

Statistic	XDH	XO	XDH	
			Fe-edge	Fe-peak
d-Spacing, Å	25–2.1	25–2.5	25–4.0	25–4.0
Wavelength	0.9790	1.0000	1.7419	1.7338
No. of unique reflections* (free)	154,198 (7,710)	51,300 (4,651)	25,562	26,217
Completeness, %	87.3	97.9	97.4	99.7
$I/\sigma(I)$	12.0	16.5	13.8	21.3
R_{cryst}* (R_{free})†	19.8 (23.8)	21.2 (27.5)		
Deviations in bond lengths, Å	0.010	0.013		
Deviations in bond angles, °	1.3	1.4		
Average B-value, Å^2	18.8	37.1		
No. of nonhydrogen atoms	22,372	10,109		
Waters	2,049	597		

*$R_{cryst} = \Sigma_{hkl} |F_{obs} - F_{calc}|/F_{obs}$, where F_{obs} and F_{calc} are the observed and the calculated structure factors, respectively, and the summation is over the reflections used for model refinement.

†R_{free} as for R_{cryst} except summed only over the reflections not used for model refinement (5.0% for XDH and 9.1% for XO).

panying the transition from the native XDH form to the XO form, a change in catalytic activity observed only in mammalian xanthine oxidoreductases, including the human and rat enzymes (3). In the following, we present the crystal structures of bovine milk xanthine oxidoreductase in its XDH form at 2.1-Å and in its XO form at 2.5-Å resolution. Comparison of the two molecular structures identifies the major changes that occur during the proteolytically induced XDH to XO transformation.

Materials and Methods

Structure Determination. The XO form of the enzyme was prepared by following the procedure of Nishino *et al.* (15) but omitting the second folate affinity chromatography step. Preparation of stable, crystallizable XDH, however, required changes to the established method of purification; replacing the standard pancreatin or butanol treatments with protease-free lipase incubation was the most important one. Further details of the purification and crystallization procedures are described elsewhere (B.T.E., K.O., C.E., M. Sato, Tomoko Nishino, E.F.P., and Takeshi Nishino, unpublished data).

We were able to grow diffraction-quality crystals of both the XDH and XO forms in complex with the inhibitor salicylate. Bovine milk XDH crystals belong to space group C2 with unit cell parameters a = 169.9 Å, b = 124.8 Å, c = 148.6 Å, and β = 90.9°, and contain two subunits in the asymmetric unit. XO crystallized in space group $C222_1$ with unit cell parameters a = 117.8 Å, b = 167.7 Å, and c = 154.5 Å, and one subunit per asymmetric unit. At 100 K, native data sets were collected from flash-frozen crystals to 2.1-Å resolution for XDH and to 2.5-Å for XO, respectively. MAD data were measured on XDH crystals at three wavelengths near the iron edge (Table 1). All data sets were processed by using DENZO and SCALEPACK (16). The structures of XDH and XO were solved by a combination of molecular replacement (MR) and anomalous phasing from the iron atoms in the Fe/S centers of XDH. An initial MR solution was obtained by using the program EPMR (17) with the XO native data and one *D. gigas* ALO subunit as a search model. As the cofactors were not included in the search model, electron density visible in the corresponding positions served as an additional indicator for the correctness of the solution. The solution for the XO crystal form gave a correlation coefficient (CC) of 0.231 and an *R*-factor (*R*) of 57.4%, whereas the average background values were CC = 0.189 and *R* = 59.0%. By using the dimer, as defined by crystal symmetry in the MR solution of XO, a significant solution for XDH was found with CC = 0.263 and *R* = 56.1%, with the average values for false solutions CC = 0.205 and *R* = 58.2%. From the MAD solution, four Fe sites could be identified with the program SOLVE (18), corresponding to the four expected Fe/S clusters in the XDH crystals. It was, however, not possible to obtain the location of individual iron atoms. Consequently, the calculated phases, based solely on the MAD information, were not of sufficient quality to allow interpretation of the electron density maps. Once the MR solutions had confirmed the sites of the Fe/S clusters and defined the orientation of the Fe/S clusters, the MAD phases could be extended to the full resolution of the data with the program SHARP (19). The final figures of merit were 0.42 for acentric and 0.38 for centric reflections. To fully use the power of the two independent sources of phase information, phase combination between the partly rebuilt and refined model and MAD phases was performed with the program SIGMAA (20). Solvent flattening and phase extension from 4.0 Å, together with 2-fold density averaging was performed in DM (21). The resulting maps allowed the tracing of approximately 1,280 residues per subunit with the program O (22). The model was further improved by using the program CNS (23) and refined to an *R*-factor of 27.3% (free *R* = 30.0%). After inclusion of 2,049 water molecules (average B-factor of 39.8 Å^2), the model of XDH was refined to an *R*-factor of 19.8% (R_{free} = 23.8%) by using noncrystallographic symmetry restraints. The refined XDH model was transferred into the XO electron density map, refined with CNS, and rebuilt by using O. The XO structure contained 597 waters (average B-factor of 51.1 Å^2) in the final model and was refined to an *R*-factor of 21.2% (R_{free} = 27.5%). Parameters for data collection and refinement are given in Table 1. Figures were prepared by using SPOCK (24) and MOLSCRIPT (25) and rendered by using RASTER3D (26).

Results and Discussion

Overall Structure. The overall dimensions of the dimeric enzyme are 155 Å × 90 Å × 70 Å (Fig. 1*A*). It has a butterfly shape with the dimer interface on the smaller side of the elongated subunits. The closest distance between atoms of cofactors from different subunits is more than 50 Å, making it very plausible that no intersubunit electron transfer takes place during catalysis. Each subunit has overall dimensions of 100 Å × 90 Å × 70 Å.

The monomer can be divided into three domains. The small N-terminal domain (residues 1 to 165) contains both iron/sulfur cofactors and is connected to the second, FAD-binding domain (residues 226 to 531) by a long segment consisting of residues 166 to 225, in which no electron density could be seen for residues 166 to 191. The FAD domain is connected to the third domain

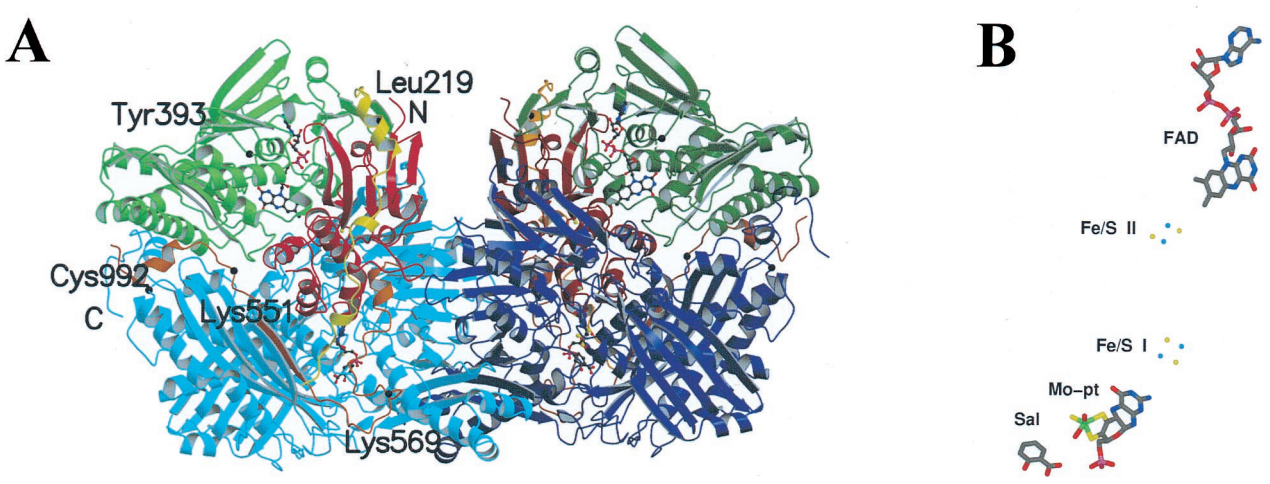

Fig. 1. (*A*) Molecular structure of the XDH dimer divided into the three major domains and two connecting loops. The two monomers have symmetry related domains in the same colors, in lighter shades for the monomer on the left and in darker shades for the monomer on the right. From N to C terminus, the domains are: iron/sulfur-center domain (residues 3–165; red), FAD domain (residues 226–531; green), and Mo-pt domain (residues 590–1,331; blue). The loop connecting the iron/sulfur domain with the FAD domain (residues 192–225) is shown in yellow, the one connecting the FAD domain with the Mo-pt domain (residues 537–589) is in brown, and the N and C termini are labeled. The FAD cofactor, the two iron/sulfur centers, the molybdopterin cofactor, and the salicylate also are included. The positions of residues discussed in the text are indicated. (*B*) For clarity, the arrangement of the cofactors and salicylate in one subunit of XDH are presented. The Mo ion is in green, the iron ions are in light blue, and the sulfur atoms in yellow.

by another linker segment (residues 532 to 589), which also is partially disordered; residues 532 to 536 could not be seen in the crystal structure. The large third domain, residues 590 to 1,332, sequesters the Mo-pterin cofactor (Mo-pt) close to the interfaces of the Fe/S- and FAD-binding domains. The C-terminal residues 1,310 to 1,331 make contacts to another molecule in the crystal lattice, rendering them clearly visible in the electron density map. In solution, however, they might well be disordered as is the C terminus in the crystal (Table 2).

The residues, which are missing in the XDH model because of insufficient density, are on the molecular surface. The C-terminal residues of the sites of pancreatin cleavage, which occurs during isolation of the XO form, Leu 219 and Lys 569 (Tomoko Nishino, unpublished results), are located in the flexible connector segments of the FAD domain. In rat XDH, trypsin cuts after Lys 184 and Lys 551, residues that are part of corresponding linker segments (3). Only the cut at Lys 551, however, causes conversion (27). This kind of mild proteolytic cleavage transforms the homodimeric XDH into a dimer of heterotrimers, a configuration of subunits identical to that of the physiologically active form of COD (14). Cys 992, one of the two amino acids modified by fluorodinitrobenzene in a reaction that causes a reversible transition between XDH and XO forms (27), is part of the Mo-pt domain. The second residue modified in this reaction is Cys 535, located in the flexible segment connecting the FAD- with the Mo-pt domain.

The Molybdopterin Domain. Although, at the present resolution, it is not possible to identify the chemical nature of atoms bound to the Mo-ion based on electron density alone, previous work has identified three ligands in addition to the two pterin cofactor sulfurs (4). The exact identity of each molybdenum ligand in the XDH structure may be inferred only from previous studies of the reaction mechanism and in analogy to the Mo-center in *D. gigas* ALO (13) (Figs. 1*B* and 2). Therefore, in the oxidized form of the active enzyme, we assign a double-bonded sulfur atom, a double-bonded oxygen atom, and an oxygen atom with a single bond as ligands to the Mo ion (4). The singly bound oxygen, which is resupplied to the Mo-center from solvent water, should be transferred to the substrate during catalysis (28). In the protein preparation used for crystallization, approximately 25% of XDH prepared by using the standard protocol has an inactive Mo-pt center (B.T.E, K.O., C.E., M. Sato, Tomoko Nishino, E.F.P., and Takeshi Nishino, unpublished work) in which the sulfur has been replaced by an oxygen atom.

To protect the Mo-pt active site, 1 mM sodium salicylate was included during purification and crystallization of both enzyme forms. Salicylate previously had been shown to be an inhibitor competitive to substrates binding in the Mo active site (3, 4). In the XDH crystal structure, the salicylate molecule is bound 6.5 Å from the Mo ion in a position that we propose to overlap the binding site of larger aromatic substrates. Although salicylate itself does not bind to the Mo-pt cofactor, it blocks the approach of potential substrates toward the metal complex (Fig. 2).

The salicylate molecule is kept in place by several hydrogen bonds and electrostatic interactions. Both its carboxylate atoms are close to the guanidinium group of Arg 880 (3.0 Å and 3.1 Å); they also bind to the hydroxyl side chain of Thr 1010 (3.0 Å) and via water 230 to the carboxylate of Glu 1261. This glutamic acid–water interaction near the Mo ion had been predicted from the *D. gigas* ALO structure (12, 13). The salicylate hydroxyl forms hydrogen bonds to both the backbone amide and hydroxyl side chain of Thr 1010 (3.2 Å and 2.9 Å, respectively). The aromatic inhibitor is aligned parallel to the ring of Phe 914 at a distance of 3.5 Å, but the two aromatic rings only slightly overlap. At the same time, the phenyl ring of Phe 1009 interacts edge-on with the center of the salicylate ring with a closest approach of 3.7 Å. Based on these results, one can model the binding of bicyclic substrates, e.g., with Phe 1009 perpendicular to the six-membered ring of xanthine and Phe 914 stacking flat on top of the substrate's five-membered ring, which would then be able to form a covalent bond with one of the Mo ligands.

Table 2. Residues without corresponding electron density

XDH	XO
1–2	1
166–191	166–223
532–536	529–570
1,332	1,316–1,332

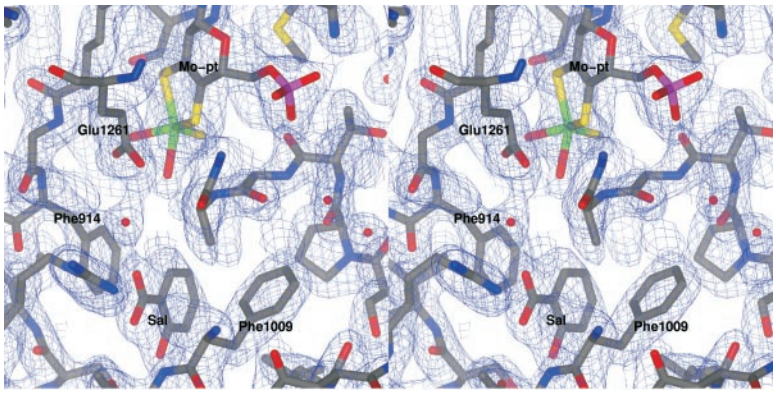

Fig. 2. Stereo representation of salicylate as bound in the Mo-pt active site of XDH plus corresponding $2F_o$–F_c electron density contoured at 1σ cutoff. Cofactor, inhibitor, the two sandwiching residues Phe 914 and Phe 1009, and Glu 1261 are labeled.

There are several well ordered water molecules in the active site but, because of the presence of salicylate and the oxidized nature of the cofactor, we do not feel confident in identifying the one supplying the oxygen for incorporation into the product (4).

The Iron/Sulfur Domain. The N-terminal domain of XDH consists of two Fe/S-cluster-binding subdomains in a structural arrangement very similar to the one found in *D. gigas* ALO (12) and *O. carboxidovorans* COD (14). The N-terminal subdomain contains an [2Fe-2S] cluster, which is coordinated to Cys 43, Cys 48, Cys 51, and Cys 73 and located in proximity to the 7α,8α-methyl groups of the flavin ring. It resembles the plant-type [2Fe-2S] ferredoxins (29). The C-terminal subdomain comprises a four-helix bundle; its cluster is coordinated to Cys 113, Cys 116, Cys 148, and Cys 150 and close to the Mo-pt group.

The two clusters are designated as Fe/S I and Fe/S II according to their distinct EPR signals. The Fe/S I signal is similar to the one shown by spinach ferredoxin and can be observed readily at temperatures up to 40 K, whereas the second signal, Fe/S II, exhibits substantially broader lines and is observable only below 22 K (4). The redox potentials for the two clusters are also different with that of Fe/S II measured as −235 mV and that of Fe/S I as −310 mV at 25°C (30). For the rat liver enzyme, the two EPR signals have been assigned to their respective sequence motifs by site-directed mutagenesis (31). The cluster bound to the unusual C-terminal —Cys—Xaa2—Cys—//—Cys—Xaa1—Cys— motif displays the Fe/S I signal, whereas the Fe/S II signal belongs to the N-terminal cluster. An equivalent assignment has been made for COD by combining EPR measurements with crystallographic results (32).

Interestingly, replacement of Cys 43, which serves as a ligand of one of the iron atoms of the Fe/S II center (iron **a** in Fig. 3) by serine results in changes of its EPR spectrum and redox potential. In contrast, a similar mutation of Cys 51, a ligand of the other iron atom (iron **b** in Fig. 3) had no effect on these features (31). The crystal structure shows iron **a** at 7.8 Å from the 7α-methyl carbon of the flavin ring and at 12.4 Å from the nearest iron atom of the Fe/S I cluster, both distances significantly shorter than those between the Cys 51-liganded iron atom **b** and the nearest atoms in the FAD and Fe/S I cofactors (8.1 Å and 14.1 Å, respectively). The distance between the Mo-ion and the nearest iron atom in the Fe/S I cluster is 14.7 Å, confirming the estimate of 14 Å based on the measurement of dipolar interaction between the two paramagnetic centers (33). The geometrical arrangements and redox potentials of these centers indicate that electrons are transferred from Mo to the two Fe/S centers in a thermodynamically favorable process. With the exception of the Mo-pt to Fe/S I interaction (van der Waals contacts between the 2-amino substituent of Mo-pt and Sγ of Cys150), there are no obvious "through-bond" pathways connecting the other cofactors. As the distances between them are shorter than 14 Å, tunneling is the most probable mechanism for electron transport (34, 35).

The FAD Domain. The FAD domain is a distant relative of a family of flavoproteins, which also contains vanillyl-alcohol oxidase (VAO) and UDP-*N*-acetylenolpyruvyl-glucosamine reductase (MurB), an enzyme involved in bacterial cell wall biosynthesis (36). The FAD-binding subunit M of COD is another member of this family. A comparison of the FAD domains of XDH and COD shows a more accurate fit when the domains are split into two subdomains after residue 413 in XDH and residue 176 in COD. When the C_α atom positions of residues 233 to 413 of XDH are compared with residues 5 to 176 of COD, they show an rms deviation of 1.4 Å. For the other half of the FAD domains (residues 414 to 526 of XDH and 177 to 285 of COD, respectively) the rms deviation is 1.7 Å. Similarity between the two domains also extends to the hydrogen-bonding pattern around

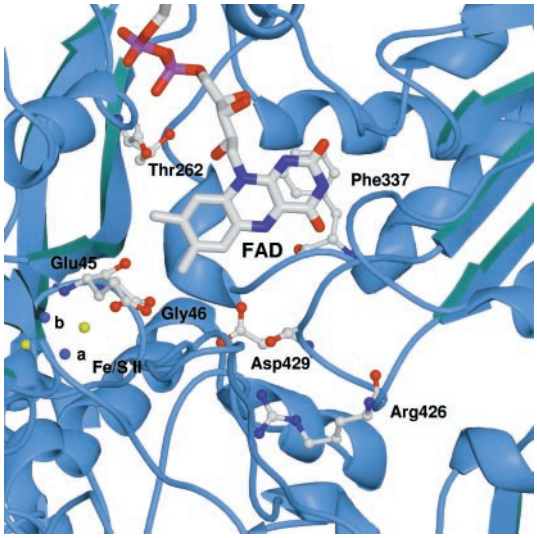

Fig. 3. FAD- and Fe/S II-binding sites of XDH. The view is into the cleft toward the *si*-site of the flavin ring. Several amino acids are drawn in ball-and-stick mode: Thr 262, Glu 45, and Gly 48, whose main chain carbonyl atoms are close to the 7α- and 8α-methyl groups of the flavin ring; Phe 337 in stacking interaction with the *re*-side of the pyrimidine part of the flavin ring; Asp 429, whose side chain lies in plane with the flavin and only 3.6 Å from its C6 atom; Arg 426, whose side chain becomes the one closest to the flavin ring in XO.

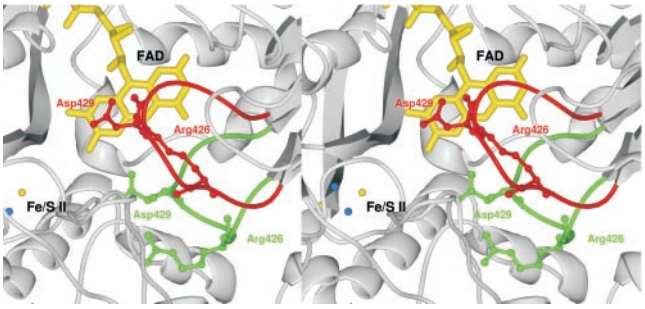

Fig. 4. Stereo representation of the change in conformation shown by an active site loop (Gln 423—Lys 433) on the XDH to XO transition; the green orientation represents the conformation it adopts in XDH and the red trace follows its path in XO. The positions of the side chains of Asp 429 and Arg 426 are indicated; they show dramatic shifts and are the major contributors to the change in electrostatic charge at the flavin site shown in Fig. 5. The view is similar to the one in Fig. 3.

the pyrimidine part of the isoalloxazine ring although the position of the flavin ring in COD is tilted into the binding pocket when compared with XDH. FAD binds in an extended conformation in a deep cleft and its isoalloxazine ring is highly solvent-accessible on the *si*-face. There is enough space for an NAD molecule to orient its nicotinamide ring parallel to the isoalloxazine. Affinity labeling of residue Tyr 419 in chicken XDH using fluorosulfonylbenzoyladenosine interferes with NAD binding (37). The corresponding residue in bovine XDH, Tyr 393, is located close to the surface of the FAD-binding cleft (Fig. 1*A*), and it is easy to imagine how addition of a bulky group to its ring could block NAD binding. Despite granting easy access to its FAD cofactor, XDH displays a relatively low oxygen reactivity. Stabilization of the flavin neutral semiquinone in the enzyme matrix has been invoked to explain this fact (3).

On the *re*-side of the flavin cofactor, the side chain of Phe 337 undergoes a π–π interaction with the pyrimidine part of the isoalloxazine ring. The residues corresponding to Phe 337 in bovine milk XDH are conserved as such in all known xanthine oxidoreductases, whereas the aromatic amino acid is replaced by a leucine in bovine ALO, an enzyme constitutively in its oxidase form. It should also be noted that the negatively charged side chain of Asp 429 is only 3.6 Å from C6 of the flavin, with no direct charge compensation nearby. Only several water molecules surround Asp 429; they in turn bind to backbone carbonyls of the Fe/S II binding loop. This general electrostatic effect could be increased through rather short contacts between the 7α- and 8α-methyl groups of the isoalloxazine ring and several backbone carbonyls (Fig. 3). The 8α-methyl carbon is 3.5 Å from the carbonyl of Thr 262 and 3.3 Å from the carbonyl of Glu 45; the 7α-methyl carbon is 3.2 Å from the carbonyl of Gly 46. Glu 45 and Gly 46 belong to the tight loop binding the Fe/S II center and separating the Fe/S cluster from the flavin ring.

Comparison of the XDH and XO Forms. The most obvious difference between the electron density maps of XDH and XO are the much longer stretches of polypeptide chain missing in the XO map (Table 2), e.g., amino acids 529 to 570, which, in XDH, comprise an α-helix, a β-strand, and a loop, together spanning a distance of approximately 70 Å (Fig. 1*A*). Although we attribute the missing density in the XDH crystal structure to mobility of the corresponding residues (the enzyme runs as a single band in SDS gels), it is conceivable that in the XO form, given its proteolyzed nature, the missing amino acids are actually removed from the protein molecule. Experiments to test this hypothesis are necessary.

The global folds of XDH and XO remain very similar, and no significant changes at or around the two Fe/S centers and the Mo-pt center are observed. The rms deviation in C_α positions between the combined Fe/S domains and Mo-pt domains of XDH and XO is 0.34 Å for 889 C_α atoms. The general conservation of structure is consistent with kinetic studies, which show no major difference between the two enzyme forms for the binding and catalysis of substrates at the Mo-pt center (3).

The reversible conversion of XDH to XO can be achieved by modification of Cys 535 and Cys 992 (27, 38). The C_α atoms of Cys 992 and residue 537 (the one closest to Cys 535 and still visible in the electron density map of XDH) are 15.7 Å apart. The formation of a disulfide bond, one possible mechanism of transformation, would therefore clearly require a conformational change. A more thorough structural interpretation of the oxidative XDH/XO transformation will have to wait until diffraction-quality crystals of the cysteine-modified protein are available.

Tryptic proteolysis of XDH after Lys 551 (4) or pancreatin cleavage after Leu 219 and Lys 569 (Tomoko Nishino, unpublished results) will result in irreversible transformation to XO. The XO molecules in our crystals have been generated by pancreatin proteolysis and should therefore be cut after Leu 219 and Lys 569. Both these amino acids assume well defined positions in XDH. In XO, however, they are part of two extended pieces of chain that are either highly flexible or absent (Table 2).

The FAD active site is the part of the enzyme that shows the largest changes when XDH is converted to XO (2, 3). It is therefore somewhat surprising to find that all of the amino acids playing a role in the transformation are located on the side opposite to the entrance to the FAD domain active-site cleft. They are at least 18 Å from the flavin cofactor, making a direct

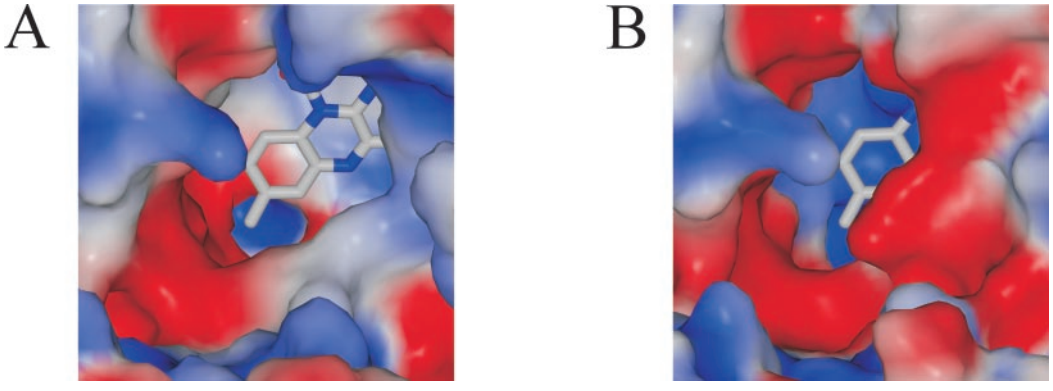

Fig. 5. The electrostatic environment looking down into the FAD binding site for XDH (*A*) and XO (*B*). The FAD molecule is shown in capped-cylinders representation. Electronegative regions are colored in red and electropositive regions in blue.

influence on the orientation of residues surrounding the FAD binding site very improbable. In XDH, however, the chain around Phe 549 gets close to the side chain of Arg 427; removal of this interaction in XO, caused by cuts to the peptide chain, could trigger the large structural rearrangement displayed by a highly charged loop (Gln 423—Lys 433) passing opposite the *si*-side of the flavin ring (Fig. 4). This transition removes the side chain of Asp 429 from its close contact with atom C6 of the flavin ring and replaces it with the side chain of Arg 426 as the flavin's closest neighbor, drastically changing the electrostatic potential of the flavin environment (Fig. 5). During this process, several residues move by as much as 20 Å from their original positions in the XDH form of the enzyme. In contrast, the structural features on the *re*-side of the flavin ring are largely undisturbed by the XDH to XO conversion, with the exception of a slight movement of the ring of Phe 337, which stacks over the pyrimidine part of flavin.

The ensuing electrostatic differences between the two forms of the enzyme strongly support previous studies that used 6- and 8-mercapto-flavins as active site probes and found that XDH shifts the pK of the ionizable substituent by more than 4 pH units (39, 40). After the Gln 423—Lys 433 loop assumes its new position, it blocks access of the substrate NAD^+ to the FAD cofactor (Figs. 4 and 5*B*). This change prevents the dehydrogenase activity without disturbing interactions between the alternate substrate, oxygen, and the isoalloxazine ring. Differences in the kinetics and the oxidation reduction behavior of XDH and XO are accounted for by the presence of a binding site for NAD^+, as well as by a substantially lower reduction potential for the $FADH\cdot/FADH_2$ couple, equivalent to a stabilization of the flavin semiquinone, in XDH, relative to XO (3, 4).

In the future, we will need to extend our analyses of XDH and XO to higher resolution with the aim of better defining the structural basis of the XDH to XO transition.

For their generous help and advice, we would like to thank the staff at Brookhaven National Laboratory beam line X8C (supported in part by a grant from MRC/NSERC), Argonne National Laboratory, BioCARS beamlines X14C and X14D, and the Photon Factory, beam line X6B (supported by the Sakabe-TARA project). Use of the Advanced Photon Source was supported by the U.S. Department of Energy, Basic Energy Sciences, Office of Science. Use of the BioCARS Sector 14 was supported by the National Institutes of Health, National Center for Research Resources. This work was supported by Grants-in-Aid for Science Research in Priority Area and a Grant-in Aid for Science Research from the Ministry of Education, Science, Sports, and Culture of Japan (to Takeshi Nishino). E.F.P. would like to thank the Protein Engineering Network of Centres of Excellence (Canada), Natural Sciences and Engineering Research Council (NSERC) and Medical Research Council (MRC) of Canada for their support. C.E. was the recipient of a postdoctoral travel grant from the Karolinska Institute, Stockholm, Sweden, and of an Ontario Cancer Institute/Amgen fellowship.

1. Schardinger, F. (1902) *Z. Untersuch. Nahrungs Genussmittel* **5,** 1113–1121
2. Massey, V. & Harris, C. M. (1997) *Biochem. Soc. Trans.* **25,** 750–755.
3. Hille, R. & Nishino, T. (1995) *FASEB J.* **9,** 995–1003
4. Hille, R. (1996) *Chem. Rev.* **96,** 2757–2816.
5. Elion, G. B. (1989) *Science* **244,** 41–47.
6. McCord, J. M. (1985) *N. Engl. J. Med.* **312,** 159–163.
7. Suzuki, H., DeLano, F. A., Parks, D. A., Jamshidi, N., Granger, D. N., Ishii, H., Suematsu, M., Zweifach, B. W. & Schmid-Schonbein, G. W. (1998) *Proc. Natl. Acad. Sci. USA* **95,** 4754–4759.
8. Olson, J. S., Ballou, D. P., Palmer, G. & Massey, V. (1974) *J. Biol. Chem.* **249,** 4363–4382.
9. Berglund, L., Rasmussen, J. T., Andersen, M. D., Rasmussen, M. S. & Petersen, T. E. (1996) *J. Dairy Sci.* **79,** 198–204.
10. Ichida, K., Ayama, Y., Noda, K., Minoshima, S., Hosoya, T., Sakai, O. Shimizu, N. & Nishino, T. (1993) *Gene* **133,** 279–284.
11. Avis, P. G., Bergel, F., Bray, R. C. & Shooter, K. V. (1954) *Nature (London)* **173,** 1230–1231.
12. Romao, M. J., Archer, M., Moura, I., Moura, J. J., LeGall, J., Engh, R., Schneider, M., Hof, P. & Huber, R. (1995) *Science* **270,** 1170–1176.
13. Huber, R., Hof, P., Duarte, R. O., Moura, J. J., Moura, I., Liu, M. Y., LeGall, J., Hille, R., Archer, M. & Romao, M. J. (1996) *Proc. Natl. Acad. Sci. USA* **93,** 8846–8851.
14. Dobbek, H., Gremer, L., Meyer, O. & Huber, R. (1999) *Proc. Natl. Acad. Sci. USA* **96,** 8884–8889.
15. Nishino, T., Nishino, T. & Tsushima, K. (1981) *FEBS Lett.* **131,** 369–372.
16. Otwinowski, Z. (1993) in *Data Collection and Processing*, eds. Sawyer, L., Isaacs, N. & Bailey, D. (Science and Engineering Research Council Darsbury Laboratory, Warrington, U.K.), pp. 52–62.
17. Kissinger, R. K., Gehlhaar, D. K. & Fogel, D. B. (1999) *Acta Crystallogr. D* **55,** 484–491.
18. Terwilliger, T. C. & Berendzen, J. (1999) *Acta Crystallogr. D* **55,** 849–861.
19. de la Fortelle, E. & Bricogne, G. (1997) *Methods Enzymol.* **276,** 472–494
20. Read, R. J. (1997) *Methods Enzymol.* **277,** 110–128.
21. Cowtan, K. D. & Main, P. (1996) *Acta Crystallogr. D* **52,** 43–48.
22. Jones, T. A., Zou, J. Y., Cowtan, S. W. & Kjeldgaard, M. (1991) *Acta Crystallogr. A* **47,** 110–119.
23. Brünger, T. A., Adams, P. D., Clore, G. M., DeLano, W. L., Gros, P., Grosse-Kunstleve, R. W., Jiang, J. S., Kuszewski, J., Nilges, M. P., Pannu, N. S., *et al*. (1998) *Acta Crystallogr. D* **54,** 905–921.
24. Christopher, J. A. (1998) SPOCK The Structural Properties Observation and Calculation Kit (The Center for Macromolecular Design, Texas A & M University, College Station, TX).
25. Merritt, E. A. & Murphy, M. E. P. (1994) *Acta Crystallogr. D* **50,** 869–873.
26. Kraulis, P. J. (1991) *J. Appl. Crystallogr.* **24,** 946–950.
27. Nishino, T. & Nishino, T. (1997) *J. Biol. Chem.* **272,** 29859–29864.
28. Xia, M., Dempski, R. & Hille, R. (1999) *J. Biol. Chem.* **274,** 3323–3330.
29. Sticht, H. & Rösch, P. (1998) *Prog. Biophys. Mol. Biol.* **70,** 95–136.
30. Hunt, J., Massey, V., Dunham, W. R. & Sands, R. H. (1993) *J. Biol. Chem.* **268,** 18685–18691.
31. Iwasaki, T., Okamoto, K., Nishino, T., Mizushima, J., Hori, H. & Nishino, T. (2000) *J. Biochem. (Tokyo)* **127,** 771–778.
32. Gremer, L., Kellner, S., Dobbek, H., Huber, R. & Meyer, O. (2000) *J. Biol. Chem.* **275,** 1864–1872.
33. Coffman, R. E. & Buettner, G. R. (1979) *J. Phys. Chem.* **83,** 2392–2400.
34. Marcus, R. A. & Sutin, N. (1985) *Biochim. Biophys. Acta* **811,** 265–322.
35. Page, C. C., Moser, C. C., Chen, X. & Dutton, L. P. (1999) *Nature (London)* **402,** 47–52.
36. Fraaije, M. W. & Mattevi, A. (2000) *Trends Biochem. Sci.* **25,** 126–132.
37. Nishino, T. & Nishino, T. (1989) *J. Biol. Chem.* **264,** 5468–5473.
38. Rasmussen, J. T., Rasmussen, M. S. & Petersen, T. E. (2000) *J. Dairy Sci.* **83,** 499–506.
39. Massey, V., Schopfer, L. M., Nishino, T. & Nishino, T. (1989) *J. Biol. Chem.* **264,** 10567–10573.
40. Hunt, J. & Massey, V. (1992) *J. Biol. Chem.* **267,** 21479–21485.